Coronavirus infection and PARP expression dysregulate the NAD Metabolome: an actionable component of innate immunity

Collin D. Heer[a,b], Daniel J. Sanderson[c,&], Lynden S. Voth[d,&], Yousef M.O. Alhammad[d,&], Mark S. Schmidt[b,&], Samuel A.J. Trammell[b,*], Stanley Perlman[e], Michael S. Cohen[c], Anthony R. Fehr[d,#], Charles Brenner[b,**,#]

[a]Free Radical and Radiation Biology Program, Department of Radiation Oncology, University of Iowa, Iowa City, IA, USA
[b]Department of Biochemistry, University of Iowa, Iowa City, IA, USA
[c]Department of Chemical Physiology & Biochemistry, Oregon Health Sciences University, Portland, OR, USA
[d]Department of Molecular Biosciences, University of Kansas, Lawrence, KS, USA
[e]Department of Microbiology & Immunology, University of Iowa, Iowa City, IA, USA

*current address: Novo Nordisk Foundation, Center for Basic Metabolic Research, University of Copenhagen, Denmark
**current address: Department of Diabetes & Cancer Metabolism, City of Hope National Medical Center, Duarte, CA USA

[&]These authors contributed equally to the work

Running title: Dysregulation of NAD metabolism by coronaviruses and PARPs

[#]**Address correspondence to:** cbrenner@coh.org and arfehr@ku.edu

Keywords: Severe acute respiratory syndrome coronavirus 2 (SARS-CoV-2), COVID-19, transcriptomics, interferon, poly(ADP-ribose) polymerase (PARP), ADP-ribosylation, nicotinamide adenine dinucleotide (NAD)

ABSTRACT

Innate immune responses are critical to control of viruses. Coronaviruses (CoVs) are positive strand RNA viruses with double-stranded RNA replication intermediates that are recognized by the innate immune system. Upon recognition, infected cells secrete interferon, which induces a set of interferon-stimulated genes that inhibit viral replication. Here we show that SARS-CoV-2 infection strikingly dysregulates the set of genes involved in consumption and biosynthesis of nicotinamide adenine dinucleotide (NAD). Highly induced genes include those encoding noncanonical poly(ADP-ribose) polymerase (PARP) family members known to function as mono ADP-ribosyltransferases but not known to deplete cellular NAD and genes encoding enzymes for salvage NAD synthesis from nicotinamide (NAM) and nicotinamide riboside (NR). We demonstrate that overexpression of PARP10 is sufficient to depress NAD levels and that the enzymatic activities of PARP10, PARP12 and PARP14 are limited by and can be enhanced by pharmacological activation of NAM salvage. We further showed that infection with the β-coronavirus murine hepatitis virus (MHV) induces a severe attack on host cell NAD^+ and $NADP^+$. Finally we show that NAMPT activation, NAM and NR dramatically decrease replication in a MHV infection model that is sensitive to PARP activity. The data show that the antiviral activities of noncanonical PARP isozyme activities are limited by their own consumption of cellular NAD and that nutritional and pharmacological interventions to enhance NAD-based defenses may boost innate immunity.

Disease attributed to the current novel coronavirus (CoV) outbreak (COVID-19) has rapidly spread globally, infecting more than 11 million people and killing > 500,000 as of early July, 2020 (1). The causative agent, severe

acquired respiratory syndrome coronavirus 2, SARS-CoV-2, is transmitted largely by aerosol and liquid droplets that infect cells of the lung epithelium (2). Like other positive strand RNA genome viruses, SARS-CoV-2 replication proceeds through formation of double-stranded (ds) RNA (3), which elicits an interferon (IFN) response (4,5). IFN proteins are secreted by infected cells to engage IFN receptors and, in an autocrine and paracrine manner, induce expression of a set of ISGs that collectively reorient cellular metabolism toward infection control by interference with transcription, translation and lipid biosynthesis (6,7).

CoV genomes do not encode enzymes needed for ATP generation, nucleotide, amino acid, lipid or protein synthesis, and therefore depend on exploitation of host functions to synthesize and assemble more viruses (3,8,9). Cellular and viral energy generation and biosynthetic programs depend on the four nicotinamide adenine dinucleotide (NAD) coenzymes, NAD^+, NADH, $NADP^+$ and NADPH, which are the central catalysts of metabolism (10). These coenzymes accept and donate electrons in essential, ubiquitous processes of fuel oxidation, lipid, nucleotide and amino acid biosynthesis, and the generation and detoxification of reactive oxygen species. The specific roles of these coenzymes in viral replication and antiviral defenses remain largely unexplored.

Among the ISGs are several members of the poly(ADP-ribose) polymerase (PARP) superfamily. These enzymes have been implicated in restriction of viral replication through mechanisms that are not well understood (11,12). PARP isozymes, except for the enzymatically inactive PARP13 protein, have an absolute requirement for NAD^+ (13,14). However, rather than using NAD^+ as an electron acceptor, PARPs consume NAD^+ in order to transfer the ADP-ribose moiety to protein side chains and/or to form ADP-ribose polymers (10). Indeed, the canonical and best characterized PARP superfamily members, PARP1 and PARP2, form poly(ADP-ribose) (PAR) largely in response to DNA damage. However, most other members of the PARP superfamily possess mono-ADP-ribosyltransfer (MARylation) activities on target proteins (13). We previously showed that murine hepatitis virus (MHV) infection strongly induces expression of noncanonical PARP isozymes PARP7, PARP9, PARP10, PARP11, PARP12, PARP13 and PARP14 (15). To determine whether these gene expression changes are incidental to MHV infection, facilitate MHV infection, or are part of an innate immune response against MHV, we treated cells with siRNAs to knock down expression of these genes and then analyzed the impact on MHV replication. Our data showed that PARP7 plays a role in facilitating replication. In contrast, PARP14 is required for full induction of IFN-β expression (15,16), suggesting PARP14 is directly involved in establishing the innate immune response in CoV infected cells.

Most CoV genomes encode 16 non-structural proteins (nsps) (3,8,9). Nsp3 contains a macrodomain, herein termed the CoV ADP-ribosylhydrolase (CARH) that removes ADP-ribosyl modifications from acidic amino acids on protein targets. Thus, CARH reverses the modification that is installed by the IFN-induced activities of MARylating PARP family members (17). CARH activity is required for virulence *in vivo* using mouse models of both MHV and SARS-CoV (17-19). Moreover, an active site mutation that ablates the ADP-ribosylhydrolase activity of CARH in MHV resulted in a virus that replicates poorly in primary bone-marrow derived macrophages (BMDMs) (15). We further identified PARP12 and PARP14 as CoV-induced ISGs that are required for the depressed replication of CARH mutant viruses, indicating that their activity is opposed by CARH-mediated reversal of ADP-ribosylation (15).

In support of the antiviral roles of IFN-induced MARylating PARP isozymes, PARP12 was shown to promote the degradation of nsp1 and nsp3 in Zika virus infection (20). PARP12 has also been shown to inhibit a wide variety of RNA viruses, including several alphaviruses, which also contain nsp3-encoded ADP-ribosylhydrolase activities (21,22). These observations suggest that key events in the innate immune response to viral infections are played out in the infected cell's NAD metabolome.

To determine whether COVID-19 disturbs NAD metabolism, we analyzed transcriptomic data from SARS-CoV-2-infected human cell lines and organoids, SARS-CoV-2-infected ferrets, and a lung biopsy from a deceased human victim of COVID-19. These data indicate that the same noncanonical PARPs induced by MHV are induced by SARS-CoV-2 and that *in vivo* infection with SARS-CoV-2

down-regulates synthesis of NAD from tryptophan and nicotinic acid (NA) while upregulating synthesis capacity from nicotinamide (NAM) and nicotinamide riboside (NR). We further show that disturbances to the NAD transcriptome scale with viral load. Though noncanonical PARP isozymes are known to use NAD^+ to MARylate target proteins, it has not been reported that they drive down cellular NAD^+. Here we show that PARP10 overexpression is sufficient to depress cellular NAD^+ and that the MARylating activities of PARP10, PARP12 and PARP14 can be pharmacologically increased by enhancing NAD salvage synthesis (salvage?) with SBI-797812 (SBI), a NAMPT activator (23).

Though the essentiality of CARH for viral function argues for cellular NAD and noncanonical PARP induction as antiviral, it remained conceivable that a depressed cellular NAD metabolome is an adaptive antiviral response to restrict viral biosynthetic processes. We therefore established a cellular system to test whether increased NAD status opposes MHV infection. Consistent with our transcriptomic analysis that CoV infection downregulates NA salvage and upregulates NAM and NR salvage, we found that NA minimally inhibited viral replication, while NAM, SBI and a clinically tested preparation of NR (Niagen)(24-26) strongly inhibit MHV replication. The data justify further analysis of how nutritional and therapeutic modulation of NAD status may potentially restrict viral infection by boosting innate immunity.

RESULTS

SARS-CoV-2 Infection of Human Lung and Enterocyte Systems Induces a Noncanonical PARP Isozyme Transcriptional Program

MHV infection in murine BMDMs launches a transcriptional program that induces transcription of noncanonical PARP isozymes PARP7, PARP9, PARP10, PARP11, PARP12, PARP13 and PARP14 by > 5-fold (15,16). To determine whether SARS-CoV-2 dysregulates the NAD system upon infection, we assembled and analyzed a set of 71 genes that encode the enzymes responsible for conversion of tryptophan, NA, NAM, and NR to NAD^+, plus the enzymes responsible for NAD(H) phosphorylation, NADP(H) dephosphorylation, NAD^+-dependent deacylation, ADP-ribosylation, cADP-ribose formation, nicotinamide methylation/oxidation, and other related functions in transport, binding, redox and regulation (**Supplementary Material 1**). We then analyzed RNAseq data from SARS-CoV-2 infection of three human lung cell lines, A549, normal human bronchial epithelia (NHBE), and Calu-3 (**Fig. 1A-C**) (27). We found that SARS-CoV-2 induces transcription of PARP9, PARP10, PARP12 and PARP14 with lesser effects on PARP7 and PARP13 in A549 cells and induces transcription of PARP9, PARP12 and PARP14 in NHBE cells (**Fig. 1A-B**). Calu-3 cells exhibit the most robust response, inducing PARP7, PARP9, PARP10, PARP12 and PARP14 more than 4-fold as well as PARP3, PARP4, PARP5a, PARP5b and PARP8 to a lesser, but statistically significant, degree (**Fig. 1C**). Based on the finding that SARS-CoV-2 infects gut enterocytes, we analyzed RNAseq data obtained from infected enterocyte organoids (28). Similar to the lung cell lines and to the transcriptional effect of MHV infection, enterocyte organoids infected with SARS-CoV-2 induce PARP9, PARP12 and PARP14 (**Fig. 1D**).

In vivo SARS-CoV-2 Infection Disturbs Noncanonical PARP Isozyme Expression and NAD Biosynthesis

Ferrets have been shown to be permissive to SARS-CoV-2 infection (29) and are being used as a system to probe host responses as well as potential preventative and therapeutic agents. To determine if PARP upregulation following SARS-CoV-2 infection is also observed *in vivo*, we probed high-quality RNAseq data from the tracheas of mock and 3-day SARS-CoV-2 infected ferrets (27) and found that the noncanonical PARP induction program is conserved in this relevant animal model (**Fig. 1E**). Specifically, PARP4, PARP5, PARP9, PARP13, PARP14 and PARP15 were all > 4-fold induced with significant but lesser induction of PARP7 and PARP11. In ferret tracheas, we observed other significant alterations to the NAD gene set. The data indicate that transcription of NMRK1 and concentrative nucleoside transporter CNT3 are induced in response to CoV infection, suggesting increased capacity for uptake and conversion of NR to NAD^+ and $NADP^+$ (30). Notably, in mouse models of damaged brain and heart, upregulation of NMRK gene expression is associated with therapeutic efficacy of NR (31)(32). Additionally, the ferret data show strongly depressed NNMT expression—by

decreasing NAM methylation, this gene expression change could promote NAM salvage (33) and the efficiency of NAD-boosting by NR or NAMPT activators (24), representing a homeostatic attempt of virally infected cells to maintain their NAD metabolome (34).

COVID19 Patient Lung Recapitulates the PARP Induction Program Seen in Ferrets and In Vitro

Finally, though ferrets are susceptible to infection by SARS-CoV-2, they do not progress to serious disease seen in humans (29). We therefore examined the NAD gene set in RNAseq data from the lung of an individual who died of COVID-19 (27). Though lacking the replicates and the synchrony of the ferret RNAseq data, the human data showed that PARP9, PARP11 and PARP13 were upregulated in the deceased individual's lung (**Fig. 1F**).

Transcriptional Dysregulation of NAD Metabolism Scales with Viral Titer

Angiotensin-converting enzyme 2 (ACE2) serves as a receptor for SARS-CoV-2 entry (35). To determine the effect of overexpression of ACE2 or greater virus exposure on the NAD transcriptome, we compared high quality RNAseq data from control or ACE2 overexpressing A549 cells infected at low (0.2) or high (2) multiplicity of infection (MOI). As shown in **Fig. 2**, greater viral exposure dysregulated more NAD related genes. The viral load-dependent changes came in three types. First, PARP7 is strongly dependent on viral load, being minimally induced in A549 cells infected at a low MOI (**Fig 2A**). However, in cells expressing ACE2 or infected at high MOI, PARP7 was one of the most highly induced PARP isozymes (**Fig. 2B-D**). Second, as ACE2 or more virus was added, transcription of more PARP superfamily members was disturbed. ACE2 and higher MOI both downregulated expression of PARP1 while they upregulated expression of 12 of the other 16 PARP isozymes. Third, on the basis of transcriptional changes, viral infection appears to alter NAD biosynthesis from tryptophan and the three salvageable NAD precursor vitamins. ACE2 and higher MOI both downregulated expression of QPRT, which is required for the conversion of quinolinate to nicotinic acid mononucleotide in the *de novo* biosynthetic pathway that originates with tryptophan. Similarly, NADSYN, which is required for synthesis of NAD from both tryptophan and NA is downregulated by viral infection, suggesting that CoV infection might disadvantage repletion of the NAD metabolome from either tryptophan or NA. In contrast, NAMPT, which is required for NAD synthesis from NAM, was consistently upregulated in SARS-CoV-2 infected cells, and NMRK1, which is required for NAD synthesis from NR, was upregulated when cells were infected at high MOI. In addition, the normally minimally expressed NR kinase gene, NMRK2, was upregulated in the ACE2 overexpressing cells infected at high MOI.

Notably, NAD biosynthetic gene changes were also conserved *in vivo* with NAMPT and NMRK1 gene expression increased by viral infection in ferrets and in the sample from the deceased person's lung. Further data on transcriptomic alterations to NAD synthesis in all nine data sets are provided in **Supplementary Material 11**.

PARP10 Overexpression is Sufficient to Depress NAD^+ Levels

It is well known that PARP1 activation by DNA damage greatly increases its catalytic activity, leading to depression of cellular NAD^+ and ATP (Cohen, 2020; Gupte, Liu, & Kraus, 2017). It is less clear whether transcriptional induction of the MARylating enzymes such as PARP10 that are induced substantially by viruses including SARS-CoV-2 might disturb cellular NAD^+. To test whether overexpression of a MARylating enzyme is sufficient to disturb the NAD metabolome, we performed targeted quantitative NAD analysis with LC-MS/MS using internal ^{13}C standards (36) on HEK 293T cells expressing either GFP or a GFP-PARP10 fusion. We found that overexpression of GFP-PARP10 significantly depressed NAD^+ compared to overexpression of GFP alone (**Fig. 3A**). We next determined if the PARP10-mediated loss in NAD^+ could be restored by increasing cytosolic NAD^+ synthesis with SBI, a small molecule activator of NAMPT, which promotes NAM salvage (23). SBI enhanced NAD^+ synthesis in GFP expressing cells, but did not significantly enhance NAD^+ in PARP10 expressing cells, indicating that PARP10 expression is sufficient to limit cellular NAD^+ (**Fig. 3A**).

Enhanced NAD Salvage Increases the Activity of PARP Isozymes Induced by SARS-CoV-2 infection

The ability of SBI to elevate cellular NAD^+ in GFP-expressing cells but not in PARP10-expressing cells suggested that overexpressed PARP isozymes are active at lower levels of cellular NAD^+ but left open the question of whether overexpressed PARP isozymes have enzymatic activities that are limited by the depressed NAD^+ status that they confer. To determine whether the activity of PARP10, PARP12 and PARP14 can be increased by NAMPT activation, we measured ADP-ribosylated protein abundance by western blot in cells overexpressing GFP, PARP10, PARP12 or PARP14 in the presence or absence of SBI. Consistent with the ability of SBI treatment to elevate cellular NAD^+, SBI enhanced PARP1 autoPARylating activity in GFP-expressing cells. SBI treatment resulted in a striking increase in PARP10 activity as evidenced by enhanced PARP10 autoMARylation. A similar result was observed with PARP12 albeit to a lesser degree. Finally, while PARP14 does not exhibit known automodification activity, SBI treatment of PARP14-expressing cells resulted in a significant increase in PARP14 target MARylation (**Fig. 3B**). These results indicate that activities of overexpressed PARP isozymes are limited by cellular NAD^+ levels and can be enhanced pharmacologically.

MHV Infection Drives Down Cellular NAD^+ and $NADP^+$ in Infected Cells

Given that divergent CoVs consistently induce members of the PARP superfamily at the mRNA level, we asked whether MHV infection alters the NAD metabolome. We infected delayed brain tumor (DBT) cells with MHV-A59 at a MOI of 3 and subjected the cells to quantitative targeted NAD metabolomics 12 hours after infection (36). Infection led to a > 3-fold depression of cellular NAD^+ and $NADP^+$ with respect to control after a mock infection (**Fig. 4A**). To address the possibility that these effects are specific to a cancer cell line and not a primary viral target cell population, we prepared bone marrow derived macrophages (BMDM) from C57BL/6 mice and infected them with MHV-A59 at a MOI of 3. Similar to DBT cells, we observed a greater than 3-fold depression of cellular NAD^+ and $NADP^+$ with respect to control cells at 12 hours (**Fig. 4B**). Thus, in primary cells that represent an authentic CoV target cell population, MHV depresses NAD coenzymes.

NAD Boosting Compounds Decrease Replication of a CARH-mutant MHV

We have previously reported that the CARH domain of MHV and SARS-CoV Nsp3 proteins is required for replication *in vivo* (17-19). Moreover, the N1347A active site mutation that ablates the ADP-ribosylhydrolase activity of CARH and *in vivo* infectivity of MHV resulted in a virus that replicates poorly in primary BMDM cells but reaches similar peak titers as WT virus in a transformed 17Cl-1 fibroblast cell line (15,18). These data suggest that a CARH inhibitor would be completely antiviral *in vivo* and would show some activity in dampening replication in cellular infection models.

Our data establish that noncanonical PARPs are consistently induced by CoV infection (**Figs. 1-2**); can depress cellular NAD^+ and have their activity limited by cellular NAD^+ (**Fig. 3**); and have known antiviral activities (20-22). These suggest that boosting cellular NAD through the transcriptionally upregulated NAMPT and NMRK pathways would have antiviral activity. However, it remained a possibility that the interferon response of infected cells evolved to drive down cellular NAD^+ in order to rob the virus of biosynthetic capacity.

To test the hypothesis that NAD-boosting interventions would depress viral replication in sensitive cellular assays, we measured MHV infection of BMDM and 17Cl-1 systems as a function of addition of NA, NAM, SBI or NR (**Fig. 5A**). As previously reported, N1347A reached similar peak titers as WT virus in 17Cl-1 cells. However, the addition of NA, NAM, SBI and Niagen NR all significantly decreased its replication (**Fig. 5B**). Consistent with increased NAMPT and NMRK gene expression and depressed NADSYN expression in SARS-CoV-2 -infected cells (**Fig. 1-2**), NAM, SBI and NR had significantly greater effects on N1347A replication than NA. NAM, SBI-797812, and NR decreased N1347A replication by 8.3, 4.4, and 6.4 fold respectively, while NA decreased its replication by only 1.9 fold (Fig. 5B). None of these treatments affected WT virus replication in 17Cl-1 cells, suggesting that increased NAD^+ levels enhance PARP isozyme-dependent MARylation activities and not other biochemical functions.

Next we tested the ability of Niagen NR to reduce N1347A replication in BMDM cells. Here, N1347A with no treatments had a

replication defect of 4.8-fold compared to WT virus, similar to our previous report (15). Consistent with the view that higher NAD^+ status depresses viral infectivity in cellular assays, addition of NR to cultured infected by N1347A further depressed replication by 2.7-fold (**Fig. 5C-D**). Recognizing that naked infection of cells with virus is much more permissive than *in vivo* infections in which CARH mutations are fully attenuated, we rely on N1347A replication for sensitivity to NAD^+ status. We also expect that cell culture conditions will be identified in which the effect of NAM, SBI and NR can be measured with wild-type viruses by introduction of oxidative and other stresses.

Overall, our data indicate that: *i)* CoV infection initiates the expression of multiple noncanonical PARP isozymes and dysregulates other genes involved in NAD metabolism; *ii)* CoV infection and PARP10 expression can dramatically decrease NAD^+ accumulation; and *iii)* NAD^+ boosting agents can improve PARP isozyme function and decrease replication of a CoV that is sensitive to MARylating activities.

DISCUSSION

SARS-CoV-2 is a highly infectious agent that constitutes a significant threat to public health (2). Morbidity and mortality data make it clear that age, smoking status and multiple preexisting conditions greatly increase the frequency of serious illness and death (37). There is an abundance of data from model systems and humans that age and conditions of metabolic stress including obesity and type 2 diabetes (38), smoking (39), heart failure (32), nerve damage (40) and central brain injury (31) challenge the NAD system in multiple affected tissues. Though PARP1 was known to be a significant consumer of NAD^+, we showed that noncanonical PARP isozymes are consistently upregulated by CoV infections, that PARP10 overexpression can depress the NAD metabolome and that three noncanonical PARP isozymes that are induced by SARS-CoV-2 have MARylating activities that are limited by cellular NAD status. While the degree of depression of the NAD metabolome is surely sensitive to time and MOI, the >3-fold depression seen in this study is precedented in human immunodeficiency virus and Herpes virus infections (41,42).

Though the genetic requirement for CARH for viral replication *in vivo* (15,17-19) strongly suggested that higher NAD^+ status would be protective and this is consistent with the potentially higher NAD^+ status of people who successfully fight off COVID-19 disease (37), it was also conceivable that IFN and PARP-mediated cellular repression of the NAD metabolome constituted a mechanism for cells to deprive the virus of anabolic capacity. However, here we showed that boosting NAD^+ through the NR and NAMPT pathways depresses replication in a highly susceptible cellular infection model.

This result warrants *in vivo* testing. We suggest that the three most translationally important tests are: inhibition of SARS-CoV-2 in animal infection models; challenge of healthy people with the common cold-causing CoV 229E (43); and a standard of care +/- NAD-boosting trial for COVID-19 patients with acute respiratory distress syndrome that monitors disease outcome and the storm of inflammatory cytokines (44). Significantly, in a small placebo-controlled clinical trial designed to address the oral safety and activity of Niagen NR in older men, it was discovered that 1 gram of NR per day depresses levels of IL-6, IL-5, and IL-2 (26), suggesting the possibility that Niagen or other NAD boosters could help manage inflammation and disease due to COVID-19 in addition to enhancing the initial innate immune response to viral replication. Similar approaches might also be tested in the context of other viral infections that induce noncanonical PARP isozymes and/or encode viral ADP-ribosylhydrolase activities (21,22).

Based on gene expression data in response to SARS-CoV-2 infection (**Fig. 1-2**), NAD boosting approaches involving increased *de novo* or NA-dependent synthesis are unlikely to be strongly effective because they require expression of genes such as QPRT, NADSYN and NAPRT (45) that are depressed by SARS-CoV-2 infection. Consistent with gene expression changes, in the cellular infection system, we showed that addition of NA only modestly reduced virus replication (**Fig. 5B-C**, **Table 1**).

Based on gene expression data as well as MHV cellular infection data, NAM, NAMPT activators and NR have similar potential to be strongly protective *in vivo*. However, there are a few caveats. First, that at pharmacological doses, NAM has the potential to function as a PARP inhibitor (46). Second, NAMPT is considered a driver of pulmonary vascular remodeling and potentially a target to be inhibited to maintain

lung health of some people at risk for COVID-19 (47). Thus, in order to maximize the likelihood of success in human CoV prevention and treatment trials, care should be taken to carefully compare efficacy and dose-dependence of NR, SBI, NAM with respect to control of cytokine storm and antiviral activities *in vivo*.

While caution should be exercised with respect to any preventative measure, NAD boosting approaches have the potential to support the innate immune system and address the age-, smoking- and comorbid conditions associated with worse SARS-CoV-2 outcomes (37). The potential societal benefit of a safe and readily available molecule to support prevention and public health is hard to overstate, especially as new outbreaks of COVID-19 emerge.

EXPERIMENTAL PROCEDURES

RNASeq analysis—Sequence counts for **Fig. 1-2** including cell lines, ferrets, and human subjects infected with SARS-CoV-2 (strain USA-WA1/2020) were derived from published RNAseq (27). Genes with Status = Low or Outlier were not considered for analysis. The Calu-3, A549 (high MOI), A549-ACE2 (low and high MOI), ferret and human data were obtained from data set GSE147507. Data were analyzed using DESeq2 to calculate fold change and p-values (see **Code Availability**). Enterocyte data were obtained from published RNAseq (28). Genes with a p-value of zero were treated as having a p-value equal to the next lowest p-value in that dataset. Genes with $p > 0.05$ ($-\log(p) > 1.30$) were considered statistically significant. Graphs were generated using GraphPad Prism v8.

Cell culture—DBT, 17Cl-1, HEK293T, and HeLa cells expressing the MHV receptor carcinoembryonic antigen-related cell adhesion molecule 1 (a gift from Dr. Thomas Gallagher, Loyola University, Chicago, IL) were grown in Dulbecco's modified Eagle medium (DMEM) supplemented with 10% fetal bovine serum (FBS), HEPES, sodium pyruvate, non-essential amino acids, L-glutamine, penicillin and streptomycin. To create BMDMs, bone-marrow cells were harvested from C57BL/6 mice and differentiated by incubating cells with 10% L929 cell supernatants and 10% FBS in Roswell Park Memorial Institute (RPMI) media for seven days. Cells were washed and replaced with fresh media every day after the 4th day. For analysis of the NAD metabolome HEK293T cells were transfected with 1µg of pEGFP-C1 Empty Vector or pEGFP-C1-CMV-PARP10 using CalPhos Mammalian Transfection Kit (Takara Bio). 6 hours later the cells were treated with chemical treatments in DMEM + 10% FBS at 37˚C 5% CO_2 for 18h.

Mice—Animal studies were approved by the University of Kansas Institutional Animal Care and Use Committee (IACUC) as directed by the Guide for the Care and Use of Laboratory Animals (Protocol #252-01). Anesthesia or euthanasia were accomplished using ketamine/xylazine. Pathogen-free C57BL/6 mice were purchased from Jackson Laboratories and maintained in the animal care facility at the University of Kansas.

Virus infection—Recombinant WT (rJIA -GFPrevN1347) and N1347A (rJIA -GFP-N1347A) MHV were previously described (Fehr et al. 2015). Both viruses expressed eGFP. MHV-A59 was previously described (48). All viruses were propagated on 17Cl-1 as previously described (Grunewald 2019). DBT, 17Cl-1, and BMDM cells were infected as described in the figure legends with a 1-hour adsorption period, before virus was removed from the well and replaced with fresh media. For NAD analysis, DBT cells were washed with PBS and replenished with serum-free DMEM prior to infection with no supplements except penicillin and streptomycin and were maintained in serum-free media throughout the infection. For treatments with NAD modulating compounds, 10 µM NA, NAM, and SBI-797812 were added immediately following the adsorption phase. For NR experiments, 100 nmole of NR was added to cells in 24 well plates in serum-free media 4 hr prior to infection, removed during the adsorption phase, then another 100 nmol NR in serum free media was added following the adsorption phase. Another 100 nmol of NR was then added directly to the media again at 12 hpi. Cells and supernatants were collected at 18 hpi and viral titers were determined by plaque assay.

Quantitative NAD metabolomics—NAD metabolites were quantified against internal standards in two LC-MS/MS runs as described (36).

Western Analysis of PARP MARylation—HEK293T were transfected with 3µg pEGFP-C1 empty vector, pEGFP-C1-CMV-PARP10, pEGFP-C1-CMV-PARP12, or pEF1-EGFP-C1-

PARP14[553-1801] via CalPhos Mammalian Transfection Kit. 6 hours later the cells were treated with chemical treatments in DMEM + 10% FBS at 37˚C 5% CO_2 for 18h. Cells were washed in PBS and lysed in 50 mM HEPES pH 7.4, 150 mM NaCl, 1mM $MgCl_2$, 1 mM TCEP, 1% Triton X-100 with the addition of Protease Inhibitors (Roche), 30 μM rucaparib (Selleck), and 1 μM PDD0017273 (Sigma). Lysates were microcentrifuged for 15 min at 4˚C, quantified by Bradford assay, and supernatants were transferred to new tube with 4x SDS sample loading buffer (0.2M Tris-HCl pH 6.5, 4% BME, 8% w/v SDS, 0.0.8% Bromophenol Blue, 40% Glycerol). Samples were resolved via SDS-PAGE and transferred to nitrocellulose. Blots were blocked with 5% Milk-PBST for 30 min, incubated O/N in primary antibody (Rabbit Pan-ADPr 1:1000, Cell Signaling E6F6A; Rabbit GFP 1:1000, Chromotek PABG1-100; Mouse Tubulin 1:1000; Cell Signaling DM1A). Primary incubation was followed with HRP-conjugated secondary antibodies (Rabbit-HRP 1:10000, Jackson Laboratories 111-035-144; Mouse-HRP 1:5000, Invitrogen 62-6520). Blots were developed by chemiluminescence and imaged on a ChemiDoc MP system (Bio-Rad). Blot analysis was performed in Image-Lab (Bio-Rad).

PARP Plasmids. pEGFP-C1-CMV-PARP10, pEGFP-C1-CMV-PARP12, or pEF1-EGFP-C1-PARP14[553-1801] were generated with standard restriction digest cloning.

Data and code availability. Transcriptomic data for all NAD related genes is provided in Supplementary Materials 2-10. Primary RNAseq data are from GSE147507 (27)(28). NAD metabolomics data are provided in Supplementary Materials 12-14. Code for the generation of data in Supplementary Materials 4 and 6-10 is provided.

SUPPLEMENTARY MATERIALS

1. NAD gene list
2. Differential gene expression for Figure 1A
3. Differential gene expression for Figure 1B
4. Differential gene expression for Figure 1C
5. Differential gene expression for Figure 1D
6. Differential gene expression for Figure 1E
7. Differential gene expression for Figure 1F
8. Differential gene expression for Figure 2B
9. Differential gene expression for Figure 2C
10. Differential gene expression for Figure 2D
11. NAD synthesis gene expression summarized Supplemental Materials 2-10.
12. NAD metabolomics for Figure 3A
13. NAD metabolomics for Figure 4A
14. NAD metabolomics for Figure 4B

AUTHOR CONTRIBUTIONS

ARF, MSC and CB designed the experiments. YMOA, LSV, and DJS performed experiments with ARF and MSC, respectively. SAJT and MSS obtained NAD metabolomic data with CB. SP provided expertise. CDH performed informatic analyses with CB. Data were analyzed by all authors. The manuscript was written by CB with assistance of ARF, MSC and CDH.

ACKNOWLEDGMENTS

We thank Stephen Gardell for kind gift of SBI-797812, ChromaDex for Niagen, Michael Chimenti and Henry Keen for informatic support, and Noah Fluharty and Grant Welk for assistance in graphing and statistics. Work was supported by NIH grants HL147545 (CB), GM008629 (SAJT), GM113117 and AI134993 (ARF), AI060699 and AI091322 (SP), CA245722 (CDH), 1NS08862 (MSC), Roy J. Carver Trust (CB), and Pew Charitable Trusts (MSC).

Competing Interests

CB is chief scientific adviser of ChromaDex and owns shares of ChromaDex stock. CB, SAJT, SP and ARF applied for a patent on uses of NAD boosting compounds to protect against CoVs. Others declare no competing interests.

REFERENCES

1. Dong, E., Du, H., and Gardner, L. (2020) An interactive web-based dashboard to track COVID-19 in real time. *Lancet Infect Dis*
2. Wu, D., Wu, T., Liu, Q., and Yang, Z. (2020) The SARS-CoV-2 outbreak: what we know. *International journal of infectious diseases : IJID : official publication of the International Society for Infectious Diseases*
3. Fehr, A. R., and Perlman, S. (2015) Coronaviruses: an overview of their replication and pathogenesis. *Methods Mol Biol* **1282**, 1-23
4. Totura, A. L., and Baric, R. S. (2012) SARS coronavirus pathogenesis: host innate immune responses and viral antagonism of interferon. *Curr Opin Virol* **2**, 264-275
5. Kindler, E., Thiel, V., and Weber, F. (2016) Interaction of SARS and MERS Coronaviruses with the Antiviral Interferon Response. *Adv Virus Res* **96**, 219-243
6. Schoggins, J. W., and Rice, C. M. (2011) Interferon-stimulated genes and their antiviral effector functions. *Curr Opin Virol* **1**, 519-525
7. Channappanavar, R., Fehr, A. R., Zheng, J., Wohlford-Lenane, C., Abrahante, J. E., Mack, M., Sompallae, R., McCray, P. B., Jr., Meyerholz, D. K., and Perlman, S. (2019) IFN-I response timing relative to virus replication determines MERS coronavirus infection outcomes. *J Clin Invest* **130**, 3625-3639
8. Zhu, N., Zhang, D., Wang, W., Li, X., Yang, B., Song, J., Zhao, X., Huang, B., Shi, W., Lu, R., Niu, P., Zhan, F., Ma, X., Wang, D., Xu, W., Wu, G., Gao, G. F., Tan, W., China Novel Coronavirus, I., and Research, T. (2020) A Novel Coronavirus from Patients with Pneumonia in China, 2019. *N Engl J Med* **382**, 727-733
9. Wu, C., Liu, Y., Yang, Y., Zhang, P., Zhong, W., Wang, Y., Wang, Q., Xu, Y., Li, M., Li, X., Zheng, M., Chen, L., and Li, H. (2020) Analysis of therapeutic targets for SARS-CoV-2 and discovery of potential drugs by computational methods. *Acta Pharm Sinica B* **in press**
10. Belenky, P., Bogan, K. L., and Brenner, C. (2007) NAD+ metabolism in health and disease. *Trends in Biochemical Sciences* **32**, 12-19
11. Alhammad, Y. M. O., and Fehr, A. R. (2020) The Viral Macrodomain Counters Host Antiviral ADP-Ribosylation. *Viruses* **12**
12. Fehr, A. R., Singh, S. A., Kerr, C. M., Mukai, S., Higashi, H., and Aikawa, M. (2020) The impact of PARPs and ADP-ribosylation on inflammation and host-pathogen interactions. *Genes Dev* **34**, 341-359
13. Cohen, M. S. (2020) Interplay between compartmentalized NAD(+) synthesis and consumption: a focus on the PARP family. *Genes Dev* **34**, 254-262
14. Gupte, R., Liu, Z., and Kraus, W. L. (2017) PARPs and ADP-ribosylation: recent advances linking molecular functions to biological outcomes. *Genes Dev* **31**, 101-126
15. Grunewald, M. E., Chen, Y., Kuny, C., Maejima, T., Lease, R., Ferraris, D., Aikawa, M., Sullivan, C. S., Perlman, S., and Fehr, A. R. (2019) The coronavirus macrodomain is required to prevent PARP-mediated inhibition of virus replication and enhancement of IFN expression. *PLoS Pathog* **15**, e1007756
16. Grunewald, M. E., Shaban, M. G., Mackin, S. R., Fehr, A. R., and Perlman, S. (2020) Murine Coronavirus Infection Activates the Aryl Hydrocarbon Receptor in an Indoleamine 2,3-Dioxygenase-Independent Manner, Contributing to Cytokine Modulation and Proviral TCDD-Inducible-PARP Expression. *Journal of virology* **94**
17. Fehr, A. R., Channappanavar, R., Jankevicius, G., Fett, C., Zhao, J., Athmer, J., Meyerholz, D. K., Ahel, I., and Perlman, S. (2016) The Conserved Coronavirus Macrodomain Promotes Virulence and Suppresses the Innate Immune Response during Severe Acute Respiratory Syndrome Coronavirus Infection. *mBio* **7**
18. Fehr, A. R., Athmer, J., Channappanavar, R., Phillips, J. M., Meyerholz, D. K., and Perlman, S. (2015) The nsp3 macrodomain promotes virulence in mice with coronavirus-induced encephalitis. *Journal of virology* **89**, 1523-1536
19. Eriksson, K. K., Cervantes-Barragan, L., Ludewig, B., and Thiel, V. (2008) Mouse hepatitis virus liver pathology is dependent on ADP-ribose-1"-phosphatase, a viral function conserved in the alpha-like supergroup. *J Virol* **82**, 12325-12334

20. Li, L., Zhao, H., Liu, P., Li, C., Quanquin, N., Ji, X., Sun, N., Du, P., Qin, C. F., Lu, N., and Cheng, G. (2018) PARP12 suppresses Zika virus infection through PARP-dependent degradation of NS1 and NS3 viral proteins. *Sci Signal* **11**
21. Atasheva, S., Akhrymuk, M., Frolova, E. I., and Frolov, I. (2012) New PARP gene with an anti-alphavirus function. *J Virol* **86**, 8147-8160
22. Atasheva, S., Frolova, E. I., and Frolov, I. (2014) Interferon-stimulated poly(ADP-Ribose) polymerases are potent inhibitors of cellular translation and virus replication. *J Virol* **88**, 2116-2130
23. Gardell, S. J., Hopf, M., Khan, A., Dispagna, M., Hampton Sessions, E., Falter, R., Kapoor, N., Brooks, J., Culver, J., Petucci, C., Ma, C. T., Cohen, S. E., Tanaka, J., Burgos, E. S., Hirschi, J. S., Smith, S. R., Sergienko, E., and Pinkerton, A. B. (2019) Boosting NAD(+) with a small molecule that activates NAMPT. *Nat Commun* **10**, 3241
24. Trammell, S. A., Schmidt, M. S., Weidemann, B. J., Redpath, P., Jaksch, F., Dellinger, R. W., Li, Z., Abel, E. D., Migaud, M. E., and Brenner, C. (2016) Nicotinamide riboside is uniquely and orally bioavailable in mice and humans. *Nat Commun* **7**, 12948
25. Dollerup, O. L., Christensen, B., Svart, M., Schmidt, M. S., Sulek, K., Ringgaard, S., Stodkilde-Jorgensen, H., Moller, N., Brenner, C., Treebak, J. T., and Jessen, N. (2018) A randomized placebo-controlled clinical trial of nicotinamide riboside in obese men: safety, insulin-sensitivity, and lipid-mobilizing effects. *The American journal of clinical nutrition* **108**, 343-353
26. Elhassan, Y. S., Kluckova, K., Fletcher, R. S., Schmidt, M. S., Garten, A., Doig, C. L., Cartwright, D. M., Oakey, L., Burley, C. V., Jenkinson, N., Wilson, M., Lucas, S. J. E., Akerman, I., Seabright, A., Lai, Y. C., Tennant, D. A., Nightingale, P., Wallis, G. A., Manolopoulos, K. N., Brenner, C., Philp, A., and Lavery, G. G. (2019) Nicotinamide Riboside Augments the Aged Human Skeletal Muscle NAD(+) Metabolome and Induces Transcriptomic and Anti-inflammatory Signatures. *Cell Rep* **28**, 1717-1728 e1716
27. Blanco-Melo, D., Nilsson-Payant, B. E., Liu, W.-C., Moller, R., Panis, M., Sachs, D., Albrecht, R. A., and tenOever, B. R. (2020) SARS-CoV-2 launches a unique transcriptional signature from in vitro, ex vivo, and in vivo systems. *Cell* **in press**
28. Lamers, M. M., Beumer, J., van der Vaart, J., Knoops, K., Puschhof, J., Breugem, T. I., Ravelli, R. B. G., Paul van Schayck, J., Mykytyn, A. Z., Duimel, H. Q., van Donselaar, E., Riesebosch, S., Kuijpers, H. J. H., Schippers, D., van de Wetering, W. J., de Graaf, M., Koopmans, M., Cuppen, E., Peters, P. J., Haagmans, B. L., and Clevers, H. (2020) SARS-CoV-2 productively infects human gut enterocytes. *Science*
29. Shi, J., Wen, Z., Zhong, G., Yang, H., Wang, C., Huang, B., Liu, R., He, X., Shuai, L., Sun, Z., Zhao, Y., Liu, P., Liang, L., Cui, P., Wang, J., Zhang, X., Guan, Y., Tan, W., Wu, G., Chen, H., and Bu, Z. (2020) Susceptibility of ferrets, cats, dogs, and other domesticated animals to SARS-coronavirus 2. *Science*
30. Bieganowski, P., and Brenner, C. (2004) Discoveries of nicotinamide riboside as a nutrient and conserved NRK genes establish a preiss-handler independent route to NAD+ in fungi and humans. *Cell* **117**, 495-502
31. Vaur, P., Brugg, B., Mericskay, M., Li, Z., Schmidt, M. S., Vivien, D., Orset, C., Jacotot, E., Brenner, C., and Duplus, E. (2017) Nicotinamide riboside, a form of vitamin B3, protects against excitotoxicity-induced axonal degeneration. *FASEB J* **31**, 5440-5452
32. Diguet, N., Trammell, S. A. J., Tannous, C., Deloux, R., Piquereau, J., Mougenot, N., Gouge, A., Gressette, M., Manoury, B., Blanc, J., Breton, M., Decaux, J. F., Lavery, G., Baczko, I., Zoll, J., Garnier, A., Li, Z., Brenner, C., and Mericskay, M. (2018) Nicotinamide Riboside Preserves Cardiac Function in a Mouse Model of Dilated Cardiomyopathy. *Circulation* **137**, 2256-2273
33. Neelakantan, H., Brightwell, C. R., Graber, T. G., Maroto, R., Wang, H. L., McHardy, S. F., Papaconstantinou, J., Fry, C. S., and Watowich, S. J. (2019) Small molecule nicotinamide N-methyltransferase inhibitor activates senescent muscle stem cells and improves regenerative capacity of aged skeletal muscle. *Biochem Pharmacol* **163**, 481-492
34. Brenner, C. (2014) Metabolism: Targeting a fat-accumulation gene. *Nature* **508**, 194-195
35. Hoffmann, M., Kleine-Weber, H., Schroeder, S., Kruger, N., Herrler, T., Erichsen, S., Schiergens, T. S., Herrler, G., Wu, N. H., Nitsche, A., Muller, M. A., Drosten, C., and Pohlmann, S. (2020) SARS-CoV-2 Cell Entry Depends on ACE2 and TMPRSS2 and Is Blocked by a Clinically Proven Protease Inhibitor. *Cell* **181**, 271-280 e278
36. Trammell, S. A., and Brenner, C. (2013) Targeted, LCMS-based Metabolomics for Quantitative Measurement of NAD(+) Metabolites. *Comput Struct Biotechnol J* **4**, e201301012
37. Yang, J., Zheng, Y., Gou, X., Pu, K., Chen, Z., Guo, Q., Ji, R., Wang, H., Wang, Y., and Zhou, Y. (2020) Prevalence of comorbidities in the novel Wuhan coronavirus (COVID-19) infection: a

systematic review and meta-analysis. *International journal of infectious diseases : IJID : official publication of the International Society for Infectious Diseases*

38. Trammell, S. A., Weidemann, B. J., Chadda, A., Yorek, M. S., Holmes, A., Coppey, L. J., Obrosov, A., Kardon, R. H., Yorek, M. A., and Brenner, C. (2016) Nicotinamide Riboside Opposes Type 2 Diabetes and Neuropathy in Mice. *Scientific reports* **6**, 26933
39. Kunzi, L., and Holt, G. E. (2019) Cigarette smoke activates the parthanatos pathway of cell death in human bronchial epithelial cells. *Cell Death Discov* **5**, 127
40. Liu, H. W., Smith, C. B., Schmidt, M. S., Cambronne, X. A., Cohen, M. S., Migaud, M. E., Brenner, C., and Goodman, R. H. (2018) Pharmacological bypass of NAD(+) salvage pathway protects neurons from chemotherapy-induced degeneration. *Proc Natl Acad Sci U S A* **115**, 10654-10659
41. Murray, M. F., Nghiem, M., and Srinivasan, A. (1995) HIV infection decreases intracellular nicotinamide adenine dinucleotide [NAD]. *Biochem Biophys Res Commun* **212**, 126-131
42. Grady, S. L., Hwang, J., Vastag, L., Rabinowitz, J. D., and Shenk, T. (2012) Herpes simplex virus 1 infection activates poly(ADP-ribose) polymerase and triggers the degradation of poly(ADP-ribose) glycohydrolase. *J Virol* **86**, 8259-8268
43. Reed, S. E. (1984) The behaviour of recent isolates of human respiratory coronavirus in vitro and in volunteers: evidence of heterogeneity among 229E-related strains. *J Med Virol* **13**, 179-192
44. Mehta, P., McAuley, D. F., Brown, M., Sanchez, E., Tattersall, R. S., Manson, J. J., and Hlh Across Speciality Collaboration, U. K. (2020) COVID-19: consider cytokine storm syndromes and immunosuppression. *Lancet* **395**, 1033-1034
45. Bogan, K. L., and Brenner, C. (2008) Nicotinic acid, nicotinamide, and nicotinamide riboside: A molecular evaluation of NAD + precursor vitamins in human nutrition. *Annual Review of Nutrition* **28**, 115-130
46. Rankin, P. W., Jacobson, E. L., Benjamin, R. C., Moss, J., and Jacobson, M. K. (1989) Quantitative studies of inhibitors of ADP-ribosylation in vitro and in vivo. *J Biol Chem* **264**, 4312-4317
47. Chen, J., Sysol, J. R., Singla, S., Zhao, S., Yamamura, A., Valdez-Jasso, D., Abbasi, T., Shioura, K. M., Sahni, S., Reddy, V., Sridhar, A., Gao, H., Torres, J., Camp, S. M., Tang, H., Ye, S. Q., Comhair, S., Dweik, R., Hassoun, P., Yuan, J. X., Garcia, J. G. N., and Machado, R. F. (2017) Nicotinamide Phosphoribosyltransferase Promotes Pulmonary Vascular Remodeling and Is a Therapeutic Target in Pulmonary Arterial Hypertension. *Circulation* **135**, 1532-1546
48. Yount, B., Denison, M. R., Weiss, S. R., and Baric, R. S. (2002) Systematic assembly of a full-length infectious cDNA of mouse hepatitis virus strain A59. *Journal of virology* **76**, 11065-11078

Compound	**Fold Reduction in N1347A Viral Titer (Compound/Vehicle)**	**p value**
NA	1.9	4.4E-2
SBI	4.4	1.7E-3
NAM	8.3	6.3E-4
NR	6.4	8E-5
NR (BMDM)	2.7	<1E-6

Table 1. Impact of NAD boosting compounds on N1347A replication. The average fold reductions in viral titer of N1347A in 2 independent experiments on 17Cl-1 or BMDM cells. The p values are from an unpaired two-tailed t-test of data from both experiments combined.

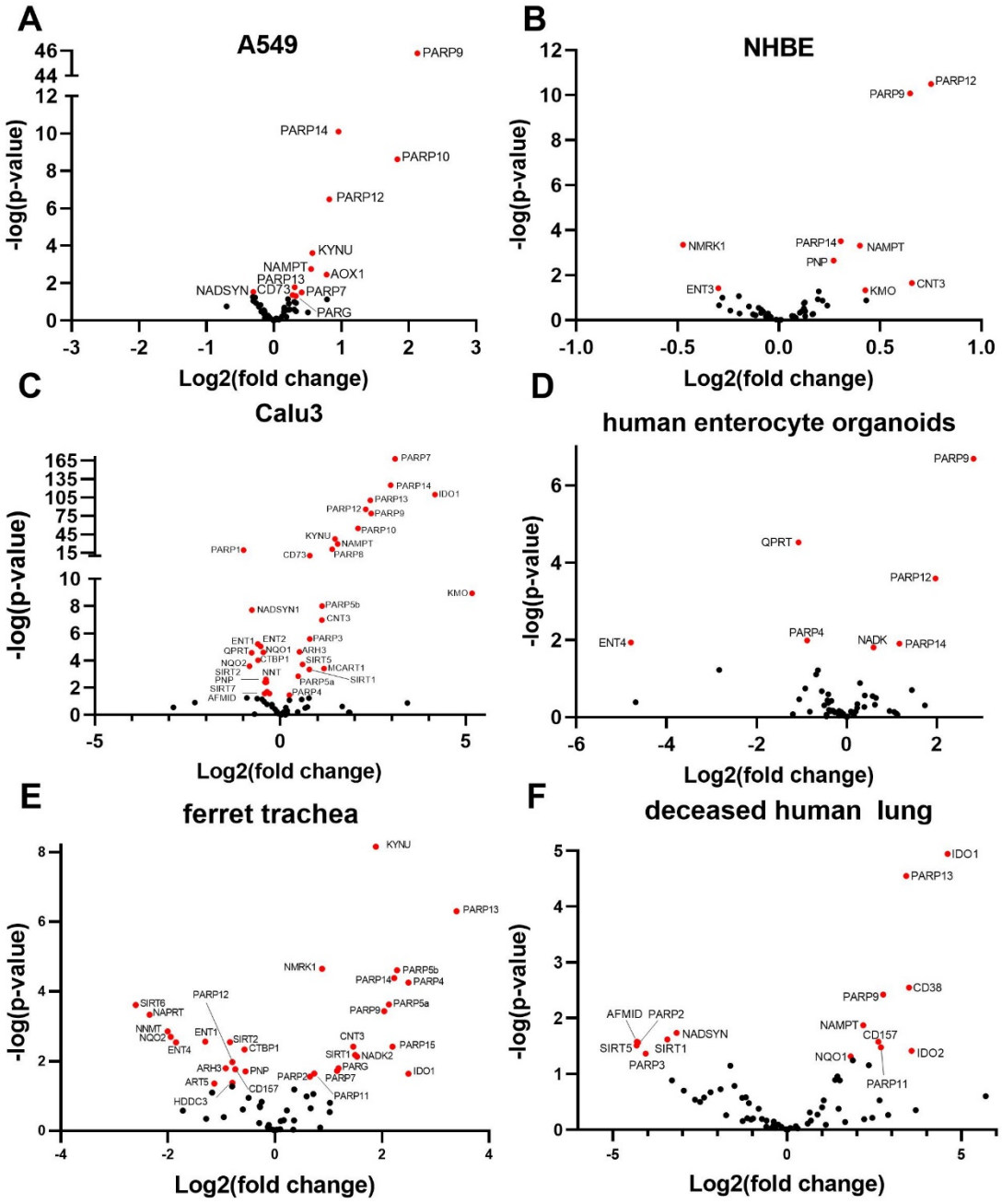

Figure 1. SARS-CoV-2 dysregulates the NAD gene set *in vitro* and *in vivo*. Differential expression analysis was performed on RNAseq data with respect to a 71 gene set representing the NAD transcriptome (Supplementary Table 1). Depicted are Volcano Plots representing normalized relative expression versus -log(P) with respect to mock infected in A) human A549 lung cancer cells (MOI = 0.2) B) NHBE cells (MOI = 2), C) Calu-3 cells (MOI = 2), D) expanding enterocytes, E) ferret trachea infected with SARS-CoV-2 and F) lung of a diseased COVID-19 patient versus a control lung sample. Further information is available in Supplementary Materials 2-7.

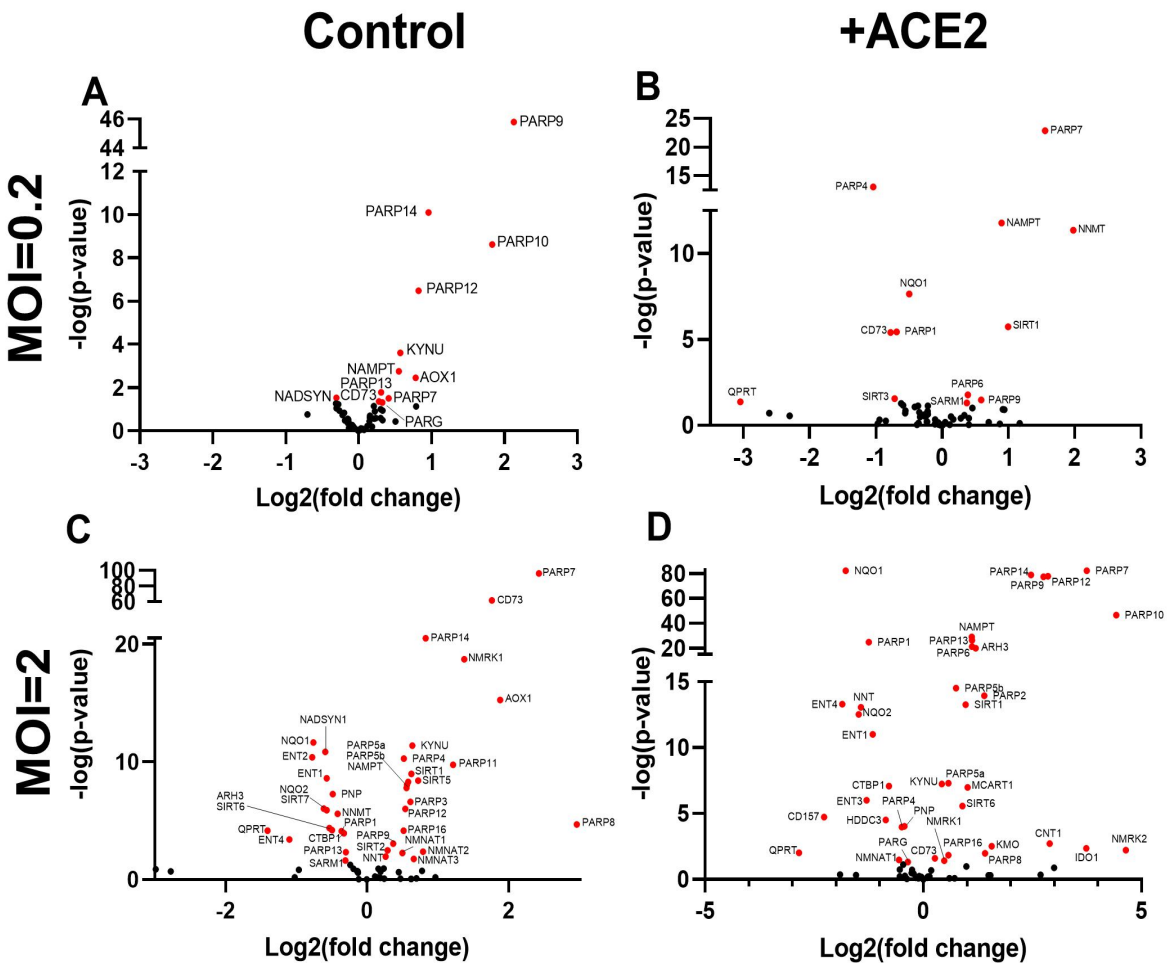

Figure 2. NAD gene dysregulation is a function of viral load. Differential expression analysis was performed on RNAseq data with respect to mock infected in A,C) Control A549 or B,D) ACE-2 overexpressing A549 cells infected with SARS-CoV-2 at a A,B) MOI = 0.2 or C,D) MOI = 2. Further information is available in Supplementary Materials 2 and 8-10.

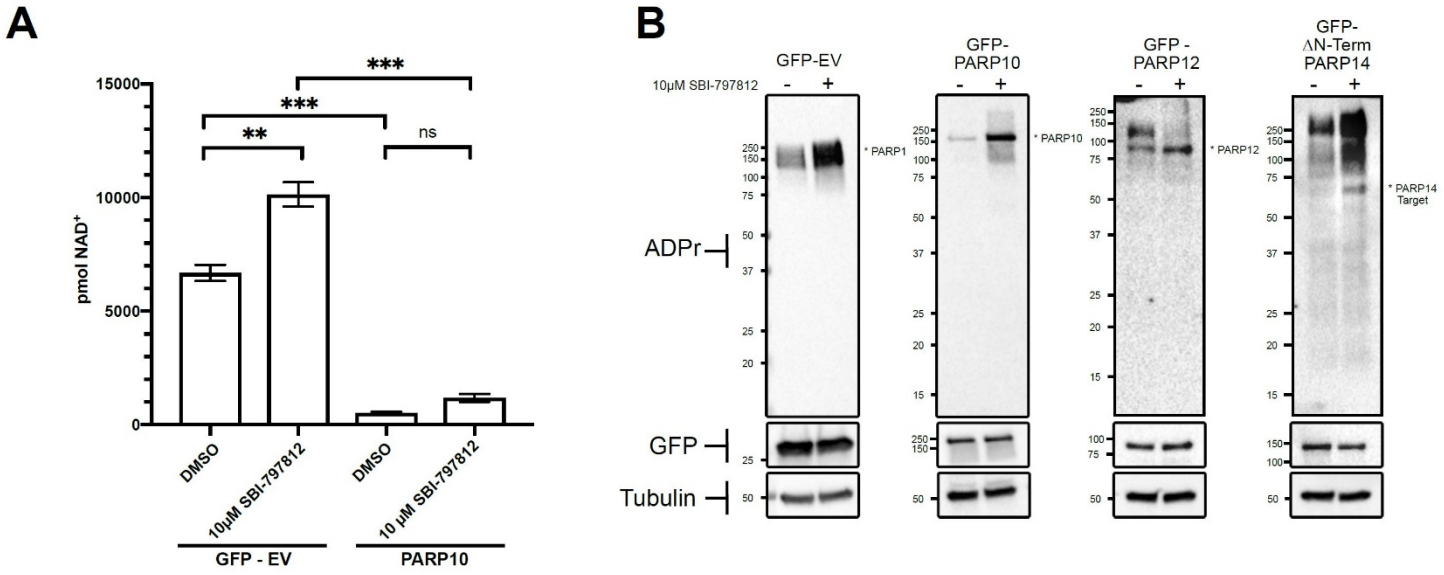

Figure 3. PARP10 overexpression is sufficient to depress cellular NAD$^+$ levels while SBI enhances activities of overexpressed PARP10, PARP12 and PARP14. A) HEK 293T cells were grown with the indicated expression plasmids for GFP or PARP10 and treated with NAMPT activator (10 μM SBI). n = 3 for each group. Error bars represent SEM, p-values are from an unpaired two-tailed t-test. See also Supplementary Information 12. B) PARP10, PARP12, PARP14 and GFP-expressing HEK293 cells were treated with 10 μM SBI and cells were collected 18 hours later. Western blot using indicated antibodies indicate that SBI promotes PARP10, PARP12 and PARP14 activity. n=3. Representative blots of three independent experiments are shown. ** $p \leq 0.01$, *** $p \leq 0.001$

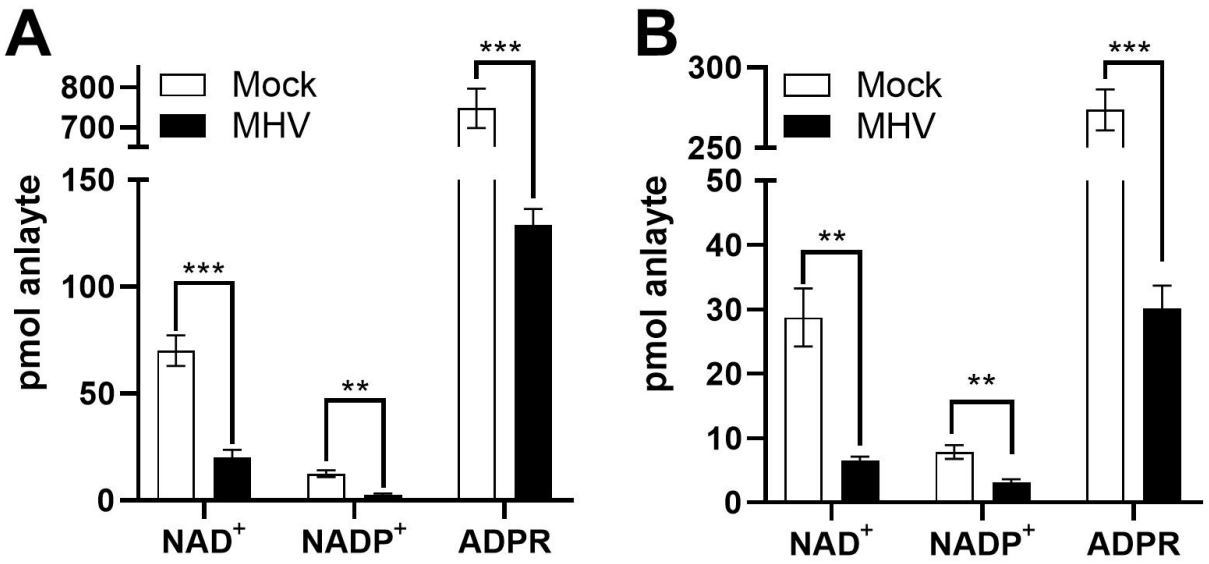

Figure 4. MHV infection disturbs the NAD metabolome. A) DBT cells and B) BMDM cells were mock infected or infected with MHV at a MOI of 3 PFU/cell and cells were collected at 12 hrs post-infection. n = 3-4 Mock; n = 4 MHV. Error bars represent SEM, p-values are from unpaired two-tailed t-test. **p ≤ 0.01, ***p ≤0 .001. See also Supplementary Materials 13-14.

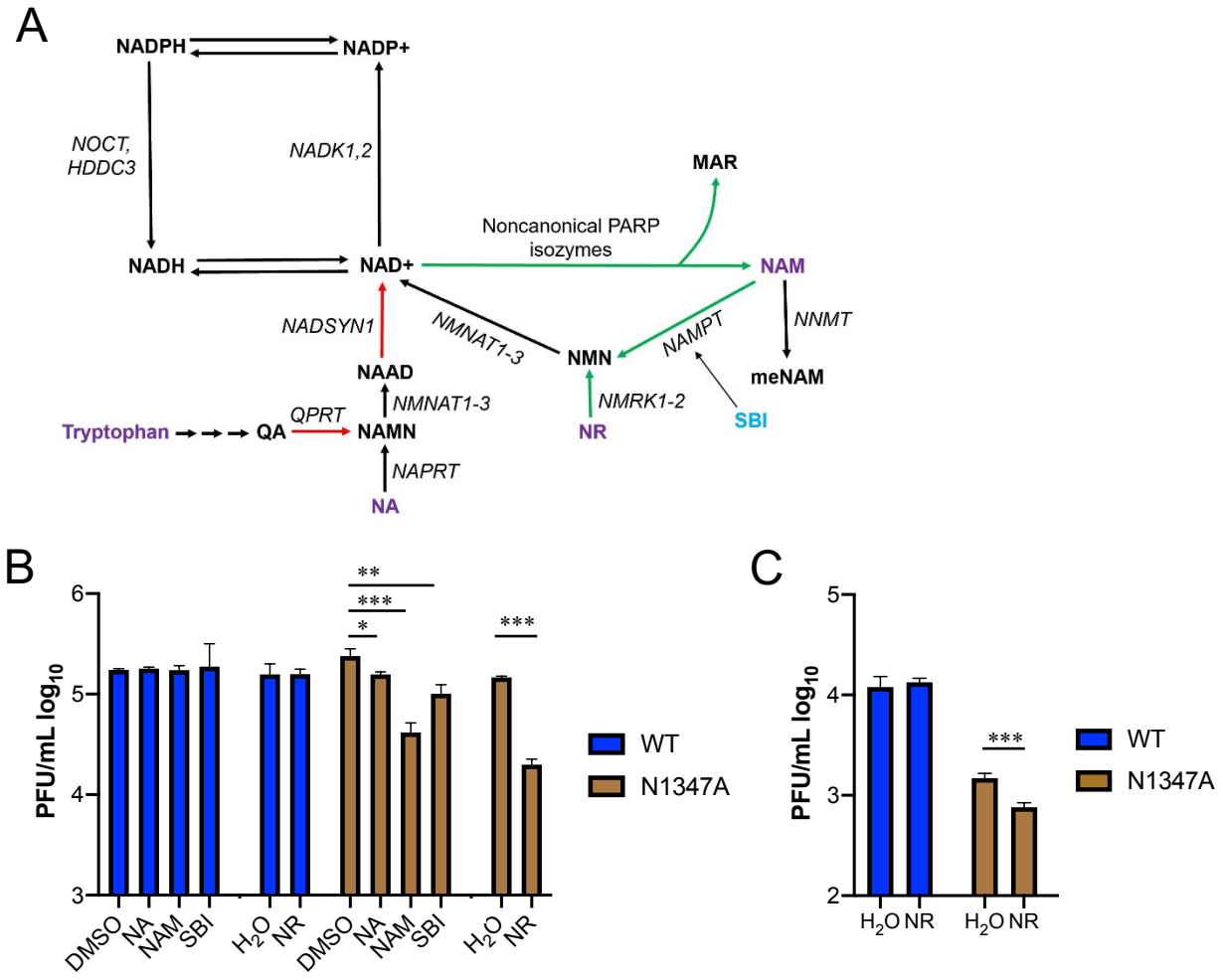

Figure 5. Boosting NAD$^+$ levels depresses replication of CARH mutant MHV. A) NAD biosynthetic pathways. Red arrows depict gene expression that is depressed by SARS-CoV-2. Green arrows depict gene expression that is increased by SARS-CoVo2. B) 17Cl-1 cells were infected with 0.1 PFU/cell WT or N1347A MHV and either mock treated (DMSO or H_2O) or treated with NA, NAM, SBI or NR as described in Methods. DMSO served as a solvent control for NAM, SBI and NA, while H_2O served as a solvent control for NR. Cells were collected at 18 hpi and analyzed for virus replication by plaque assay. Data are representative of two independent experiments, n = 3 biological replicates. C) BMDMs were infected with 0.1 PFU/cell WT or N1347A MHV and treated with H_2O or treated with NR as described in Methods. Cells were collected at 18 hpi and analyzed for virus replication by plaque assay. Data are representative of two independent experiments. n = 4 biological replicates. *p ≤ 0.05, **p ≤ 0.01, ***p≤0.001.